

In situ anomalous small angle X-ray scattering and absorption on an operating rechargeable lithium ion battery cell

Artur Braun ^{a,*}, Soenke Seifert ^b, Pappannan Thiyagarajan ^c, Stephen P. Cramer ^{d,e},
Elton J. Cairns ^{a,f}

^a Environmental Energy Technology Division, Ernest Orlando Lawrence Berkeley National Laboratory, MS 70-108B, One Cyclotron Road, Berkeley, CA 94720, USA

^b Chemistry Division, Argonne National Laboratory, 9700 S. Cass Avenue, Argonne, IL 60439, USA

^c Intense Pulsed Neutron Source Division, Argonne National Laboratory, 9700 S. Cass Avenue, Argonne, IL 60439, USA

^d Department of Applied Sciences, University of California at Davis, One Shields Avenue, Davis, CA 95616, USA

^e Physical Biosciences Division, Ernest Orlando Lawrence Berkeley National Laboratory, MS 70-108B, One Cyclotron Road, Berkeley, CA 94720, USA

^f Chemical Engineering Department, University of California at Berkeley, Gilman Street, Berkeley, CA 94720, USA

Received 11 December 2000; received in revised form 4 January 2001; accepted 4 January 2001

Abstract

We have employed anomalous small angle X-ray scattering (ASAXS) and X-ray absorption in situ on an operating lithium ion battery cell with LiMn_2O_4 as the positive electrode material. Manganese K-edge absorption spectra and scattering patterns were recorded at various stages of charge between 3.8 and 4.5 V. The shift of the manganese absorption K-edge was observed as a function of the charge of the electrode. Clear changes in the microstructure of the spinel at the 4 V plateau was observed even during the first charging cycle. © 2001 Published by Elsevier Science B.V.

Keywords: ASAXS; Microstructure; Lithium battery; In situ

PACS: 82.45.-h; 61.10.Eq; 81.40.-z; 81.40.Np; 61.72.-y; 64.60.-i

1. Introduction

The microstructure of electrodes and electrode materials is usually studied with electron microscopy (scanning electron microscopy, transmission electron microscopy). However, the application range of these techniques is limited since they probe only the local structure and generally do not permit the in situ characterization of electrodes.

In the recent years small angle X-ray scattering (SAXS) was successfully applied to study the microstructure of electrode materials for supercapacitors [1,2], batteries [3], and fuel cells [4]. SAXS allows more for a statistical global characterization of material.

We now present for the very first time results on the in situ characterization of an operating lithium ion battery cell with anomalous small angle X-ray scattering

(ASAXS). We take particular advantage of synchrotron radiation, since its tunable energy allows for anomalous scattering and thus for an element specific characterization, and since its high photon flux allows to employ in situ cells.

The cell contained LiMn_2O_4 spinel as a positive electrode and was charged and partially discharged.

Contrast variation was applied with respect to the manganese in order to study the evolution of microstructural changes in the electrode. A trimodal distribution of manganese containing objects was found. During electrochemical treatment, these objects grow irreversibly by about 50%. Also, a reversible “flip” of a superstructural Bragg reflex was observed at the point when the cell was fully charged.

2. Experimental

LiMn_2O_4 was obtained by mixing stoichiometric amounts of Li_2CO_3 and MnO_2 , subsequent firing in air

* Corresponding author. Tel.: +1-510-486-7257; fax: +1-510-486-7303.

E-mail address: abraun@lbl.gov (A. Braun).

in a furnace at 1123 K for 24 h, and cooling down under ambient atmosphere.

The spinel powder was mixed with carbon (graphite from Timcal, and Shawinigan carbon black) and binder (all together 5 wt%) and cast on an aluminum foil of 25 μm thickness and subsequently sintered at 423 K, resulting in a electrode with thickness of about 40 μm , containing spinel to about 95 wt%.

Electrodes with a diameter of 25 mm were punched from the foil sheet and vacuum dried for another 24 h and then kept under argon, before used as electrodes.

One such electrode, one Celgard 3401 separator, electrolyte (LiPF_6 dissolved in dimethyl carbonate) and a lithium foil as a counter electrode (125 μm thick) were assembled in an in situ cell, which was sealed against contamination of cell interior with air and humidity.

The in situ cell was made from two stainless steel plates with 3 mm thickness and 12 cm diameter. Each plate had concentric groves for BUNA O-rings to allow for proper sealing of the electrode/electrolyte compartment. The 5 mm \times 1.8 mm wide X-ray windows at the center of each plate were closed with beryllium plates of 380 μm thickness. The X-ray transmission of the cell in operation at 6500 eV X-ray energy was about 50%.

The experiments were carried out at the Advanced Photon Source in Argonne National Laboratory (Beamline 12 ID, BESSRC CAT). The cell was assembled in a helium filled glovebox, cabled to a portable potentiostat and data acquisition system and mounted at the ASAXS setup. As a special protective for the in situ experiment during operation, we wrapped the cell in a commercial household “ziploc” plastic bag and filled it with helium. Even 40 h after cell assembly, the cell interior was not dried out, and the lithium, spinel electrode and the electrolyte did not show any changes in color or signs of corrosion.

One half charge cycle was performed at current densities not exceeding 50 $\mu\text{A}/\text{cm}^2$, and potentials not exceeding 5 V. The charging was interrupted when the cell exhibited an open circuit potential of about 4.3 V, which was reached after 1833 min. Thereafter, the cell was discharged at 50 $\mu\text{A}/\text{cm}^2$ for another 500 min. During electrochemical treatment, ASAXS patterns (0.1 s/pattern) were recorded at particular stages of charge at 20 different energies which covered the Mn K-edge at 6545 eV and at energies in the vicinity of the absorption edge. A CCD camera was used as a position sensitive X-ray detector. Prior to each ASAXS pattern, a XANES was measured in the range between 6529 and 6575 eV, with an energy resolution of 0.1 eV (7 min/spectrum).

For the determination of the imaginary part of the atomic form factor of manganese, f'' , a XANES between 6400 and 6700 eV was recorded.

3. Results and discussion

Fig. 1 shows the charge of the spinel electrode as a function of the charging time, obtained by integration of the current during charging and discharging. After the electrode was charged, a maximum charge of 88.8 mA min was verified. Since the mass of the oxide was about 9.25 ± 1.25 mg, its average capacity was 160 ± 21.6 mAh/g. The lower limit of this value matches the theoretical capacity of 148 mAh/g fairly well. After that time span, the electrode potential showed the tendency to increase towards values larger than 4.3 V at even low current densities.

We therefore conclude that the electrode was primarily charged and thus almost free of removable lithium. Thereafter, the electrode was discharged for 190 min at a current of 200 μA .

Fig. 2 displays XANES spectra of the manganese K-edge for three different stages of charge of the oxide

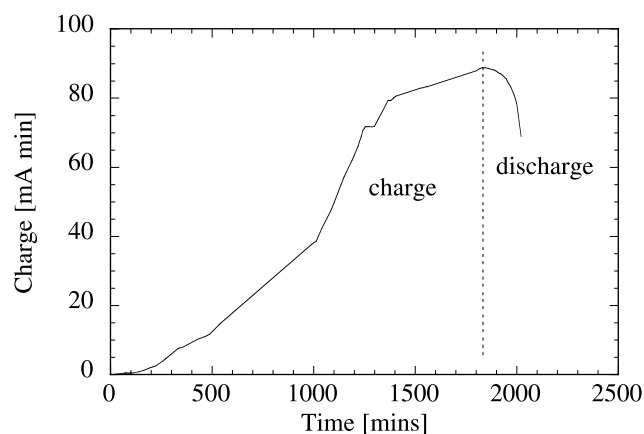


Fig. 1. Evolution of charge as a function of charging time, as obtained from integration of current.

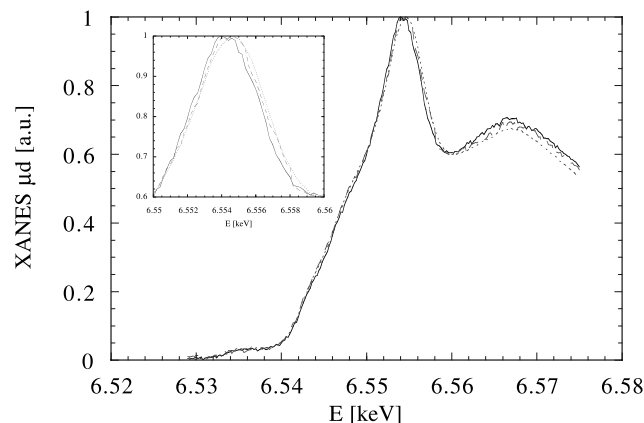


Fig. 2. XANES spectra of the sample at initial stage of charging (solid), fully charged (dotted), and after discharging (broken). The magnification of the absorption maximum in the inset shows the shift of the spectra.

electrode. While the spectra show the same overall profile, they are shifted, however, versus the energy scale (see the inset for magnification). Spectrum 1 (solid line) was obtained right at beginning of charging with the electrode being LiMn_2O_4 and the open circuit potential 3.78 V. The manganese atoms per unit cell are present with the formal charges Mn^{4+} and Mn^{3+} in equal quantities. Spectrum 2 (dotted line) was obtained when the cell was fully charged and most of the lithium in the spinel was removed, with a potential of 4.3 V. The intensity maximum of spectrum 2 is shifted by about 1.5 eV towards higher energy, compared to spectrum 1. At this stage, the manganese is mostly (to about 90%) present as Mn^{4+} . At discharging (spectrum 3, broken line), lithium is reinserted in the oxide lattice, and consequently the manganese is being reduced. Thus, spectrum 3 is shifted towards a slightly smaller energy than spectrum 2. The potential was 4.05 V. The changes in the XANES serve as a verification of the valence changes of the manganese. These findings are in line with the determination of the charge of the cell after charging.

In recent years several research groups have reported XANES spectra which show a more pronounced shift in the edge region than our spectra do. Since they also reported faster charging and discharging rates, we conclude that they had used diluted samples. Differences between their spectra and our spectra could therefore originate from different sample concentration.

Main part of the ASAXS data treatment is illustrated in Fig. 3 and will be outlined briefly. The curve with open circles (filled circles) was recorded at an energy of 6400 eV (6545 eV). The enhanced scattering of the latter curve for larger Q -values is due to the anomalous scattering of the manganese at its K-absorption edge. For the quantitative analysis of the contrast variation we applied the simplifying assumptions that (i) no correla-

tion between compositional and topological fluctuations exist and (ii) the number densities of manganese clusters and other electrode material are identical. The latter assumption is weak since we expect no metal manganese precipitations. After [5,6], we can therefore write for the entire scattered intensity

$$I^{\text{Mn}}(Q) = \frac{I(Q, E_1)}{\langle f(E_1) \rangle^2} - \frac{I(Q, E_2)}{\langle f(E_2) \rangle^2}, \quad (1)$$

Q being the scattering vector, which is related with the scattering angle Θ and the wavelength λ of the radiation used by

$$Q = \frac{4\pi}{\lambda} \sin \Theta. \quad (2)$$

Note, that by this contrast variation, we also eliminate the scattering of the in situ cell components. The atomic form factor f of manganese

$$f(E) = f_0 + f'(E) + if''(E), \quad (3)$$

was obtained using the XANES spectra and performing a Kramers–Kronig transformation. This scattering curve is marked in Fig. 3 with crosses and represents only the scattering of the manganese.

35 sets of SC were analyzed over the whole range of Li-concentration ($1 \geq (c - 1) \geq 0.1$) during electrochemical cycling.

All scattering curves recorded obey the so-called Q^{-4} -decay of the intensity for small Q very well [7]. No significant deviations from Porod's law are observed, which accounts for a smooth electron distribution.

Prior to further analysis of the scattering curves, the Porod scattering and also a constant background scattering were fitted to the data as follows:

$$I_{\text{Porod}}(Q) = c_1 + c_2 Q^{-4}. \quad (4)$$

The fit obtained is plotted as a broken line in Fig. 3 and subsequently subtracted from the scattering curve to which it was applied on. The data points (dots) in Fig. 3 represent the scattering curve which will be treated further on for object size determination. The drawn solid line in this curve is a least-square Guinier-fit, which will be discussed in the following section.

3.1. Guinier analysis

Fig. 4 displays scattering curves of the charged, uncharged, and partially discharged electrode. Each of these curves shows humps which are caused by manganese inhomogeneities in the spinel matrix. We treat the scattering within the Guinier approximation [8]. The Q -position of the inflection point of these humps yields information on the size of the objects which cause these humps. Note that by using the anomalous scattering technique it is the manganese which accounts for the features now visible in the scattering curves. It must be

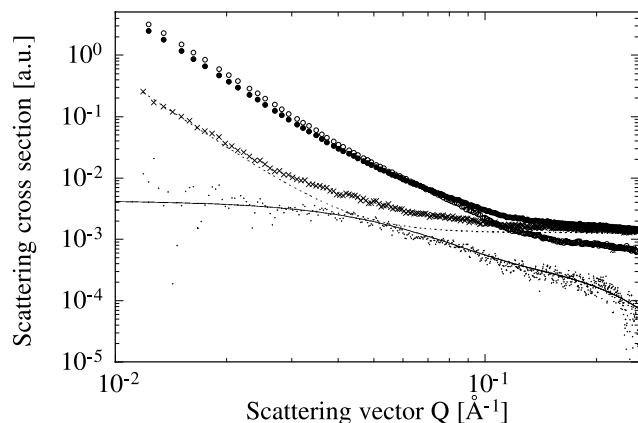


Fig. 3. Open circles (filled circles): ASAXS taken at 6400 eV (6545 eV). Crosses: Difference curve after contrast variation. Dotted line: Porod fit curve. Scattered data points: ASAXS curve after Porod subtraction. Solid line through data points: Guinier fit.

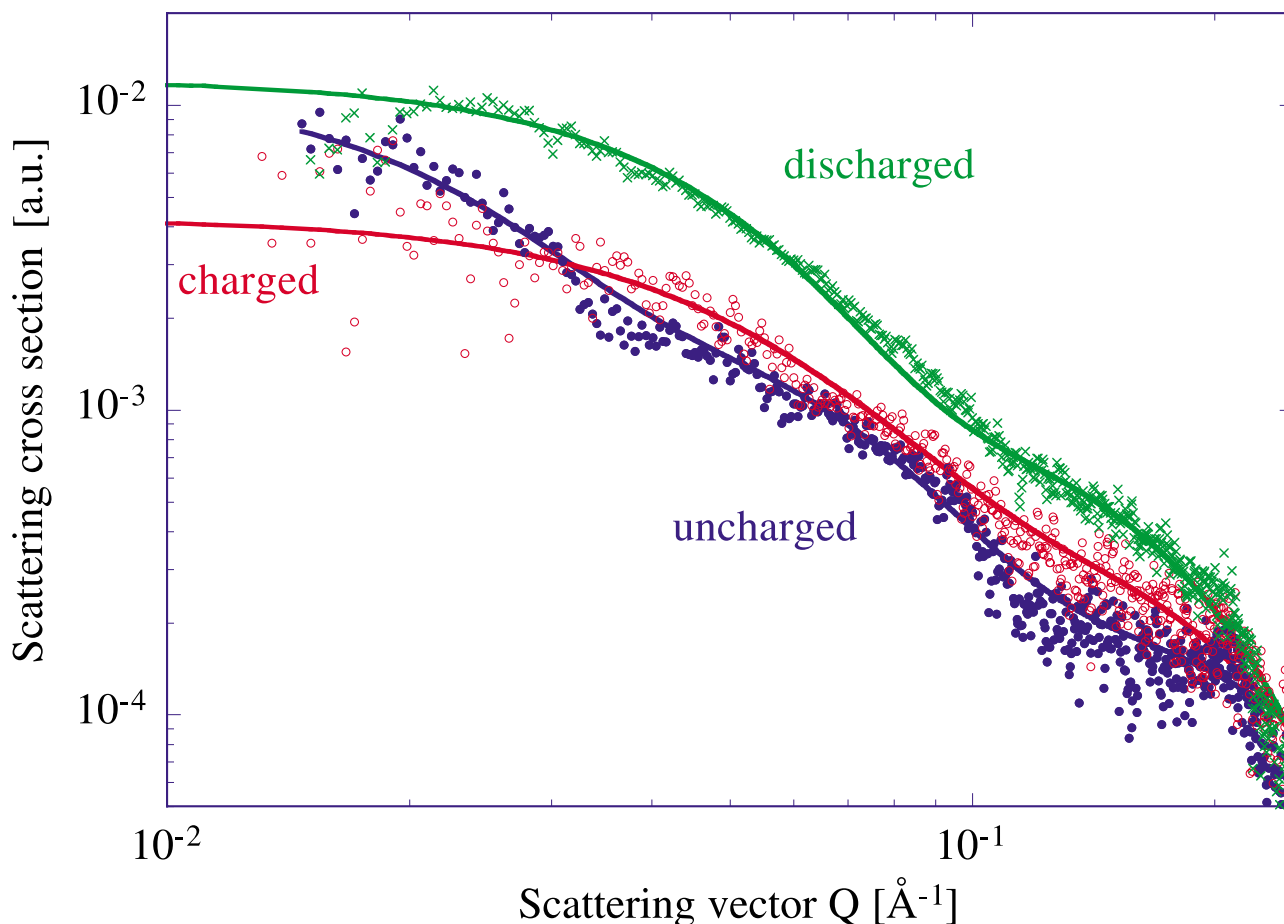


Fig. 4. Scattering curves (after contrast variation and Porod correction) with bimodal Guinier fits of uncharged (filled), charged (open) and partially discharged (crosses) samples.

kept in mind that Guinier's approximation is based on the assumption that the manganese in the spinel matrix is a diluted system. Since this requirement does not hold, a suppression of the apparent size of the objects should occur as a systematic error [8].

After Guinier [9], the structure factor of any homogeneous object can be approximated by an exponential with the *radius of gyration* R_g as the only parameter, when it is applied to the central part of the hump. The scattered intensity then reads

$$I(Q) = NV^2 \Delta n_f^2 \exp\left(-\frac{Q^2 R_g^2}{3}\right) \quad (5)$$

with N being the number of objects, V their volume, Δn_f^2 the scattering contrast and R_g being the mean square distance from the center of electron density, in analogy to the momentum of inertia in mechanics:

$$R_g^2 = \frac{\int_V \rho(r_i) r_i^2 dV_i}{\int_V \rho(r_i) dV_i}. \quad (6)$$

Another potential interpretation of the various humps would be that they are intermediate intensity maxima of

objects with a very sharp size distribution, such as in the case of spheres which were observed during the decomposition of an alloy in [5]. However, we were unable to fit an accordingly structure factor to the present experimental data. Our next observation is that the overall scattered intensity increases during delithiation. Even at re-lithiation the intensity increases, which, after Eq. (5), can be caused by either a growth of number N of objects or their volume V . Also, a change of the scattering contrast could cause a change of the intensity, for instance when the number density of Mn atoms in the material is changed.

The two humps in the scattering curves account for an at least bimodal distribution of objects. The radii of gyration are in the range 7–10 Å (nanoclusters) and 25–45 Å (mesoclusters). Qualitatively we observe that the position of the humps shifts towards lower Q -values during electrochemical treatment of the sample. This is evidence that the objects are growing, which is in line with the observed increasing overall intensity. These changes are irreversible. For a quantitative analysis, a sum of two exponentials was fitted to the experimental data as follows:

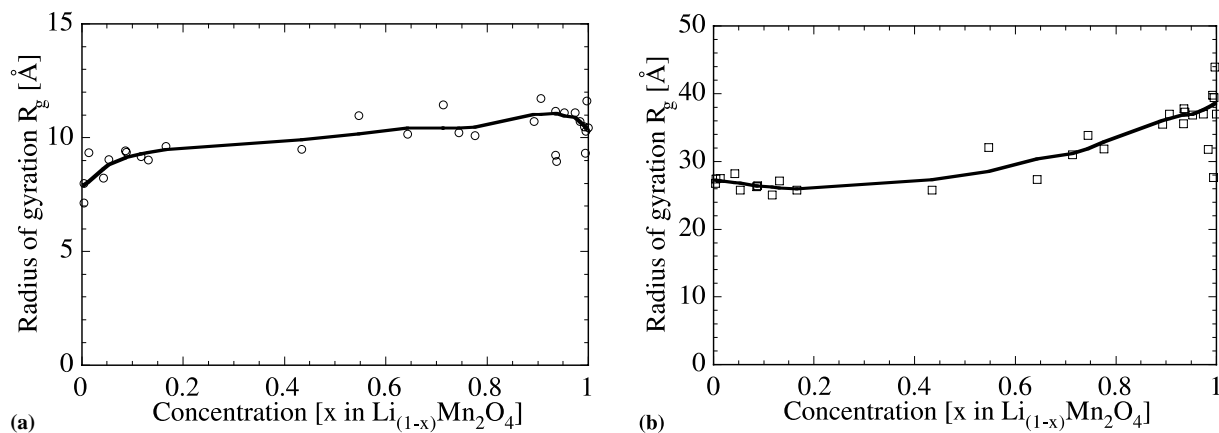


Fig. 5. (a), (b): Radii of gyration of manganese containing nanoclusters (mesoclusters) as a function of lithium concentration. Drawn lines are a guide to the eye.

$$I(Q) = a_1 \exp\left(-\frac{Q^2 R_{g,1}^2}{3}\right) + a_2 \exp\left(-\frac{Q^2 R_{g,2}^2}{3}\right). \quad (7)$$

Note that for each Guinier term a monodisperse distribution was assumed, so far.

In Fig. 5, the radii of gyration, as obtained by this least-square fitting, are plotted versus the lithium concentration in the sample. We find that both the nano- and mesoclusters are growing during electrochemical treatment. However, during initial range of charging ($0 \leq x \leq 0.1$), the mesoclusters show a slight decreasing trend, while the nanoclusters show a pronounced growth in this range.

For numerous particle shapes, relations exist for the conversion of R_g into the geometrical parameters of the bodies, provided, their shape is known. For an ellipsoid with semi-axes a , b , and c , and for a prism with edge lengths A , B , and C , following relations hold [10]:

$$R_g^2 = \frac{a^2 + b^2 + c^2}{5}, \quad (8)$$

$$R_g^2 = \frac{A^2 + B^2 + C^2}{12}. \quad (9)$$

Fig. 6 shows the SC of the uncharged and charged samples in a Kratky-plot. We found this representation most suitable to show intensity peaks which we assign to Bragg reflexions, may be reflecting a superstructure [11]. These weak peaks ($Q = 0.281 \text{ \AA}^{-1}$, 22.359 \AA) remain unchanged so far during cycling, with the exception of a major peak ($Q = 0.337 \text{ \AA}^{-1}$, 18.644 \AA), that split and shifted towards lower ($Q = 0.267 \text{ \AA}^{-1}$, 23.533 \AA) and higher Q -values ($Q = 0.302 \text{ \AA}^{-1}$, 20.805 \AA) right at the stage when the cell was fully charged. This flip of reflex was reversible, since it shifted back to its previous position right after the onset of discharging. Among 35 SC studied, only this recorded at the moment of full charge and in line with the XANES showing the cell fully charged, showed the described anomaly. Since this effect

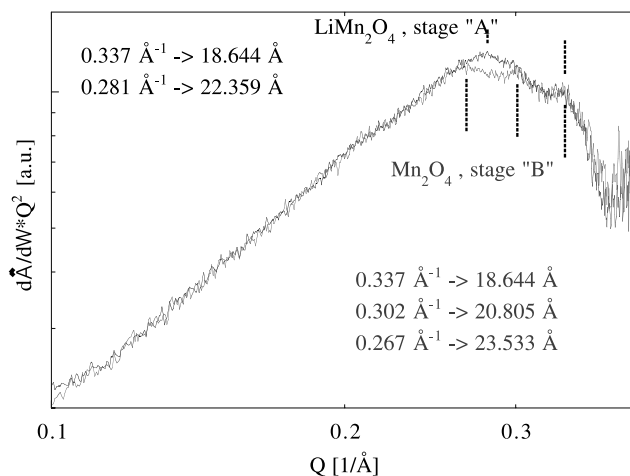


Fig. 6. Kratky plot of scattering curves of uncharged (stage A) and charged (stage B) samples.

appeared in a critically narrow window of concentration, it could maybe interpreted as a phase transition.

4. Conclusions

Microstructural changes in LiMn_2O_4 electrodes have been reported recently by various groups [11–15], including the formation of nanometer-sized antiphase-domains, superstructures, phase transformations and phase decompositions. The ASAXS data show that microstructural changes in lithium ion battery cells can be monitored in situ with these techniques. These changes occur in the spinel during (de-)lithiation even within the very first cycle at moderate currents in a safe potential range. The data obtained by Guinier analysis are probably not accurate, since the Guinier approximation is exact only to dilute systems, unless an interference function is taken into account. Therefore, the apparent Guinier radii are probably suppressed and

underestimated due to interparticle interferences. Also, it is not falsified yet whether a sharp object size distribution could cause the humps in the scattering curves. Doubtless, however, is the trend that the particles are growing during charging. This is confirmed by the monotoneous increase of the overall scattered intensity and scattering at zero angle, which is not plotted in this communication. Due to limited beamtime and a pronounced careful charging of the cell, no time was left to measure the sample at smaller Q -values and thus to resolve larger objects. We will continue these measurements and support them with additional X-ray diffraction experiments.

Acknowledgements

We are grateful to Erik Granlund (UC Berkeley, College of Chemistry) for construction of the in situ cell, Mike C. Tucker (UC Berkeley) for help with electrode manufacturing, and to Christopher Johnson (Argonne National Laboratory, CMT Division) for providing us with lithium and electrolyte on site. Helpful discussions with Günter Goerigk (Hamburger Synchrotronstrahlungslabor, Hamburg, Germany) and Erik Gullikson (Center for X-ray Optics, Lawrence Berkeley National Laboratory, Berkeley, USA) are gratefully acknowledged. Use of the Advanced Photon Source was supported by the US Department of Energy, Basic Energy Sciences, Office of Science, under Contract No. W-31-109-Eng-38. This work was supported by the Director, Office of Basic Energy Sciences, Chemical Sciences Di-

vision of the US Department of Energy, under Contract DE-AC03-76SF00098.

References

- [1] A. Braun, M. Bärtsch, B. Schnyder, R. Kötz, O. Haas, H.-G. Haubold, G. Goerigk, *J. Non-Cryst. Solids* 260 (1/2) (1999) 1–14.
- [2] A. Braun, M. Bärtsch, F. Geiger, O. Haas, R. Kötz, B. Schnyder, M. Carlen, T. Christen, Ch. Ohler, P. Unternährer, H. Desilvestro, E. Krause, in: *New Materials for Batteries and Fuel Cells*, Proceedings of the MRS, vol. 575, San Francisco, April 1999, 369 pp.
- [3] W. Xing, J.S. Xue, T. Zheng, A. Gibaud, J.R. Dahn, *J. Electrochem. Soc.* 143 (11) (1996) 3482–3491.
- [4] H.-G. Haubold, X.H. Wang, H. Jungbluth, G. Goerigk, W. Schilling, *J. Molec. Struct.* 383 (1/3) (1995) 283–285.
- [5] P. Fratzl, Y. Yoshida, G. Vogl, H.-G. Haubold, *Phys. Rev. B* 46 (1992) 11323.
- [6] G. Materlik, C.J. Sparks, K. Fischer, *Resonant Anomalous X-Ray Scattering – Theory and Applications*, North-Holland, Amsterdam, 1994.
- [7] G. Porod, *Kolloid-Z.* 124 (1951) 83.
- [8] O. Glatter, O. Kratky, *Small Angle X-Ray Scattering*, Academic Press, New York, 1982.
- [9] A. Guinier, *Ann. Phys.* 12 (1939) 161.
- [10] P. Mittelbach, *Acta Phys. Austriaca* 19 (1964) 53–102.
- [11] G. Rousse, C. Masquelier, R. Rodrigues-Carvajal, M. Hervieu, *Electrochem. Solid-State Lett.* 2 (1) (1999) 6–8.
- [12] M.M. Thackeray, et al., *Electrochem. Solid-State Lett.* 1 (1) (1998) 7–9.
- [13] M.M. Thackeray, W.I.F. David, P.G. Bruce, J.B. Goodenough, *Mater. Res. Bull.* 18 (1983) 461.
- [14] H. Wang, Y.-I. Jang, Y.-M. Chiang, *Electrochem. Solid-State Lett.* 2 (10) (1999) 490–493.
- [15] K. Kanamura, H. Naito, T. Yao, Z.-i. Takehara, *J. Mater. Chem.* 6 (1) (1996) 33–36.